PAPER

Check for updates

Two-dimensional conductive metal–organic framework with 2,3,6,7,14,15-triptycenehexathiol (TCHT) ligand: synthesis, structure, electrical conductivity and CO₂RR activity†

Wataru Murakami,[a] Taku Kitayama,[a] Yuta Chiba,[a] Haruko Moteki,[a] Risa Shirato,[a] Kazuyuki Iwase, [b] Ryojun Toyoda, [a] Ryota Sakamoto*[a] and Shinya Takaishi [*a]

Two-dimensional conductive metal–organic frameworks (2D-c-MOFs) are promising materials for applications in electrochemical devices. However, the metal sites in most 2D-c-MOFs are typically inaccessible because of π–π stacking between the 2D sheets. In contrast, 2D-c-MOFs in which the conjugated π-planes of the ligands are oriented perpendicular to the 2D sheets ("vertical ligands") can offer improved guest accessibility to the metal sites. Here, we report the synthesis of a novel vertical ligand, 2,3,6,7,14,15-triptycenehexathiol (TCHT), and its corresponding 2D-c-MOF, Cu-TCHT. Powder X-ray diffraction (PXRD) patterns suggested its honeycomb structure. Furthermore, electrochemical catalytic activity for the CO₂ reduction reaction (CO₂RR) was improved over conventional 2D-c-MOF with horizontal ligands (Cu-BHT) probably because the porous honeycomb structure with the vertical ligands facilitates access to the metal sites.

Introduction

Metal–organic frameworks (MOFs) belong to a family of porous crystalline polymers composed of metal ions and polydentate ligands.[1,2] Fundamental properties, including extensive surface area and tunable porosity, make them promising materials for gas storage,[3–5] separation,[6,7] catalysis,[8–10] chemical sensing,[11,12] *etc.* In spite of their chemical and structural diversity and flexibility, the electrically insulating nature of plenty of MOFs limit their applications for electrochemical devices. In recent years, the introduction of extended π-conjugation into the MOF skeleton has been used as one way to enhance electrical conductivity. The effective frontier orbital overlapping between ligands (pπ) and metals (dπ), as well as similar energy levels can cause long-range d–p conjugation.[13,14]

Among these, MOFs composed of π-conjugated ligands with three chelating coordination sites and transition metal ions have been actively studied because they form nanostructured sheets with two-dimensional (2D) π-conjugation extended across the plane, similar to graphene, through the hybridization of the pπ orbitals of the ligand and the dπ orbitals of the metal. Many of these MOFs use π-conjugated molecules, such as benzene or triphenylene, with oxygen, nitrogen, or sulfur atoms as coordinating atoms (Fig. 1), which is called 2D conductive MOFs (2D-c-MOFs).[15–24] These MOFs are widely applied in electrocatalysts,[25] energy storage,[26,27] and electrochemical sensors[28,29] due to their high electrical conductivity. In particular, the electrochemical conversion of CO₂ into valuable chemicals and fuels using these 2D-c-MOFs as electrocatalysts has been proposed to reduce CO₂ emissions.[30,31]

It is well known that the metal sites of transition metal ions act as active sites of the catalysts,[32–34] chemisorption,[35,36] *etc.* However, one drawback of these 2D-c-MOFs is that the π–π stacking of the two-dimensional sheets causes the metal sites to be inaccessible except on the outer surfaces. To address this issue, recent studies have focused on developing 2D c-MOFs using triptycene skeleton (Scheme 1(a)). By the combination of hexa-substituted triptycene (TCHX) and metal ions (M) that can form square planar complexes, the MX₄ plane is perpendicular to the 2D sheet, which enhances the accessibility of the guest molecules to the metal sites. Although triptycene ligands do not exhibit direct π-conjugation due to the central sp³ carbons, electrical conjugation is expected by direct orbital overlapping *via* neighboring sp² carbons (homoconjugation effect).[37–39] Recently, MOFs with oxygen or nitrogen coordination have been

ᵃDepartment of Chemistry, Graduate School of Science, Tohoku University, 6-3 Arama-ki-Aza-Aoba, Aoba-ku, Sendai 980-8578, Japan. E-mail: shinya.takaishi.d8@tohoku.ac.jp

ᵇInstitute of Multidisciplinary Research for Advanced Materials, Tohoku University, Sendai, Miyagi 980-8577, Japan
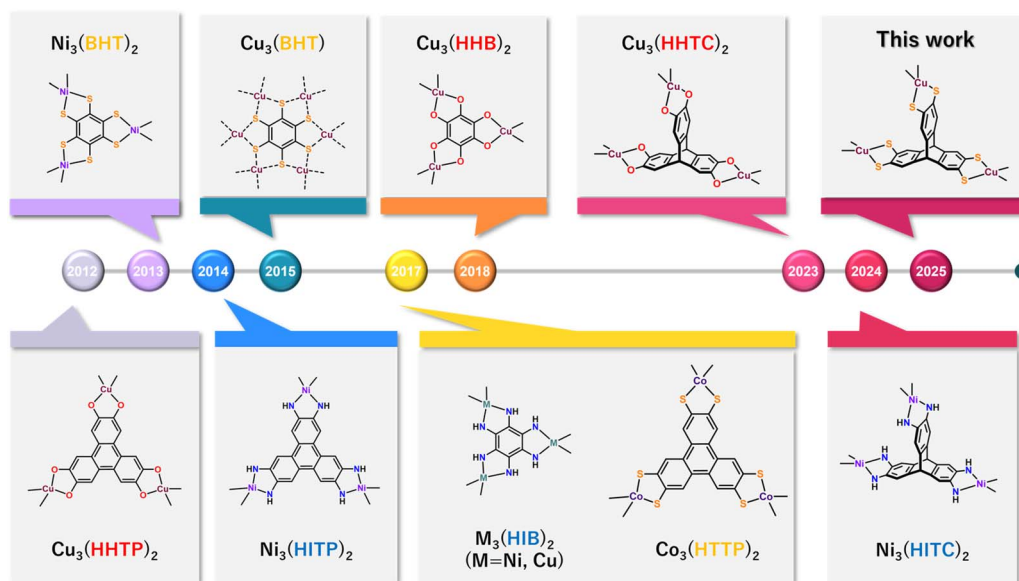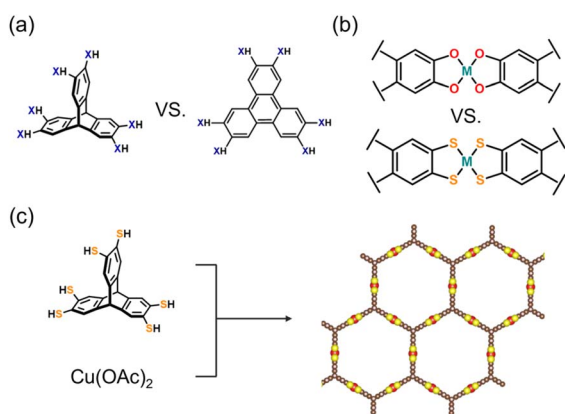
Fig. 1 Timeline of development and application of representative 2D-c-MOF.[24]

Scheme 1 (a) Comparison of vertical and horizontal ligands. (b) Comparison of a thiolate ligand against a dioxolate ligand. (c) General synthetic scheme of Cu-TCHT.

reported.[40–43] On the other hand, for sulfur coordination, the ligand itself, 2,3,6,7,14,15-triptycenehexathiol (TCHT), has not yet been reported, and consequently, therefore there is no report on a MOF comprising this ligand.

In this study, we synthesized the TCHT ligand using a novel synthetic route (Scheme 2), and also determined the single crystal X-ray structure of intact TCHT. Then, we synthesized
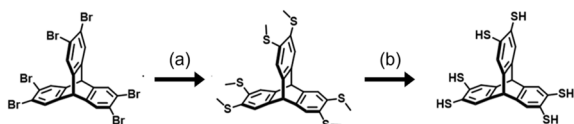
Scheme 2 Synthetic procedure for HMTTC and TCHT; (a) HBTC (0.82 mmol), CuI (5.88 mmol), and DABCO (4.0 mmol) were heated in DMSO (20 mL) at 160 °C for 15 h. (b) HMTTC (1.35 mmol) and Na (40 mmol) were reacted in liquid NH_3 (50 mL) for 3 h.

a MOF using this ligand, which showed porous honeycomb structure and semiconductive electrical conductivity. Furthermore, the MOF exhibited high electrochemical CO_2 reduction reaction (CO_2RR) catalytic activity.

Experimental

Chemicals

All the chemicals were of reagent grade, purchased from commercial sources, and used without further purification. The starting materials triptycene, benzenehexathiol (BHT), and Cu-BHT were synthesized using a previously reported procedure.[16,44,45]

Synthesis of 2,3,6,7,14,15-hexabromotripcycene (HBTC)

HBTC was synthesized using previously reported procedure with slight modifications.[46] In a 200 mL two-neck flask, triptycene (1020 mg, 4.0 mmol), anhydrous dichloromethane (20 mL), and iron powder (100 mg) were added and stirred. After cooling to −30 °C, bromine (1.35 mL, 26.2 mmol) diluted with anhydrous dichloromethane (50 mL) was added dropwise, and the mixture was stirred at −30 °C for 48 hours under the constant nitrogen flow. The generated HBr was quenched by bubbling into a saturated $NaHCO_3$ aqueous solution. During the reaction, white precipitate formed. After the reaction, the solution was quenched by adding saturated aqueous sodium sulfite solution (100 mL). The precipitate was collected by suction filtration and washed with methanol until the filtrate became colourless, and a white powder, HBTC, was obtained (1945 mg, 66.8%). ^{1}H NMR (500 MHz, $CDCl_3$): δ 7.63 (s, 6H), δ 5.24 (s, 2H).

Synthesis of 2,3,6,7,14,15-hexakis(methylthio)triptycene (HMTTC)

In a 20 mL microwave vial, HBTC (600 mg, 0.82 mmol), copper(I) iodide (1120 mg, 5.88 mmol), and 1,4-diazabicyclo[2.2.2]octane

This journal is © The Royal Society of Chemistry 2025

J. Mater. Chem. A, 2025, 13, 25724–25731 | 25725

(450 mg, 4.00 mmol) were added and ground together. Dimethyl sulfoxide (20 mL) was then added, and the reaction mixture was heated to 160 °C for 15 hours using a microwave synthesizer (Biotage Initiator+). Caution: the upper limit of the inner pressure should be set to less than 10 bar to avoid the burst of the vial, because the gas is generated during reaction. After the reaction, dichloromethane (150 mL) was added to the resulting dark red solution, which was washed three times with aqueous sodium hydroxide solution (0.35 M, 50 mL). Magnesium sulfate was added to the dichloromethane solution, which was then filtered, and the solvent was removed under vacuum to obtain a yellowish-white solid. The obtained solid was loaded onto Celite and purified using an automated flash chromatography with dichloromethane and hexane. The purified solution was dried under reduced pressure, yielding a white powder (200 mg, 43%). ^{1}H NMR (500 MHz, CDCl$_3$): δ 7.29 (s, 6H), δ 5.31 (s, 2H), δ 2.43 (s, 18H). ^{13}C NMR (126 MHz, CDCl$_3$): δ 142.9, 134.5, 123.0, 52.6, 16.8. Elemental analysis (calc. for C$_{26}$H$_{26}$S$_6$·0.2CH$_2$Cl$_2$): C, 57.44; H, 4.86; N, 0.00. Found: C, 57.45; H, 4.88; N, 0.00. APCI-MS (calc. for C$_{26}$H$_{26}$S$_6$ [M + H$^+$]): 531.04315, found: 531.04318.

Synthesis of 2,3,6,7,14,15-tripcycenehexathiol (TCHT)

The reaction was conducted under dehydrated and nitrogen atmosphere conditions, with all solutions prepared after nitrogen bubbling. A 300 mL three-neck flask was connected to a three-way stopcock linked to a manifold and a bubbler, and the remaining necks were sealed with a septum and a glass stopper. Liquid ammonia (50 mL) was collected in the flask by cooling to -78 °C while passing ammonia gas into the system. Finely chopped metallic sodium (1.1 g, 48 mmol), with the surface oxide layer removed, was added to the ammonia, forming a deep blue solution. HMTTC (980 mg, 1.35 mmol) was added, and the mixture was reacted for 3 hours. Methanol (20 mL) was then slowly added to quench the reaction, resulting in a white suspension. The suspension was stirred at room temperature, and the ammonia was evaporated. Water (20 mL) was added to the residue, followed by three washes with diethyl ether (30 mL each). Dilute hydrochloric acid (100 mL) was added, forming a white precipitate. The precipitate was filtered under reduced pressure in air, washed with water and methanol, and extracted with dichloromethane inside a nitrogen glove box. The solvent was removed under reduced pressure under anaerobic conditions to yield a white powder (490 mg, 81%). ^{1}H NMR (500 MHz, CDCl$_3$): δ 7.36 (s, 6H), δ 5.11 (s, 2H), δ 3.63 (s, 6H). Elemental analysis (calc. for C$_{20}$H$_{14}$S$_6$): C, 53.77; H, 3.19; N, 0.00. Found: C, 53.71; H, 3.43; N, 0.00.

Synthesis of Cu-TCHT

The following procedures were carried out under a nitrogen atmosphere, except for filtration process, and all solutions were nitrogen-bubbled before use. TCHT (38.0 mg, 0.086 mmol) was dissolved in dichloromethane (25 mL) and stirred. Copper(II) acetate monohydrate (50.9 mg, 0.26 mmol) in methanol (30 mL) added to the dichloromethane solution of TCHT immediately gave a brown-black solid. After stirring overnight, filtration under an atmospheric condition yielded Cu-TCHT as a black powder (53.2 mg).

Results and discussion

Syntheses of HMTTC and TCHT

TCHT was synthesized from triptycene through a three-step process (Scheme 2). Since the thiobenzyl hexasubstituted precursor could not be synthesized under the same conditions as the synthesis of BHT and HTTP, another synthetic approach was explored. HMTTC was obtained by heating hexabromo-triptycene with CuI and DABCO in DMSO and separating them by column chromatography. And then, TCHT was successfully synthesized by Birch reduction of HMTTC with metallic sodium in liquid ammonia. Both TCHT and HMTTC were characterized and identified using NMR spectroscopy and single-crystal X-ray diffraction analysis (Fig. 2, 3, S1, S2 and Tables S1, S2†).

Crystal structures of HMTTC and TCHT

Oligothiols are useful not only as ligands for coordination polymers, but also as building blocks in the construction of disulfide-based macrocycles that provide dynamic behavior.[47–51] In contrast to the importance, there are few reported examples of crystal structures of ligands with multiple dithiol ligands because it is difficult to isolate and very easily oxidized. For example, crystal structure of BHT was reported in 2023 for the first time,[45] even though the synthesis of BHT was already reported around 1990.[52,53] Here, we investigated the crystallization of HMTTC and TCHT under anaerobic conditions in order to clarify the crystal structure of the building block. As a result, each single crystal was obtained by slow-evaporation of the dichloromethane solution of HMTTC and chloroform solution of TCHC under dinitrogen atmosphere.

HMTTC and chloroform were crystallized in 1 : 1 ratio, and both were crystallographically independent (Fig. 2a). All HMTTC were axially aligned (Fig. 2b). The short contacts between non-hydrogen atoms are shown in Fig. 2c. Except for
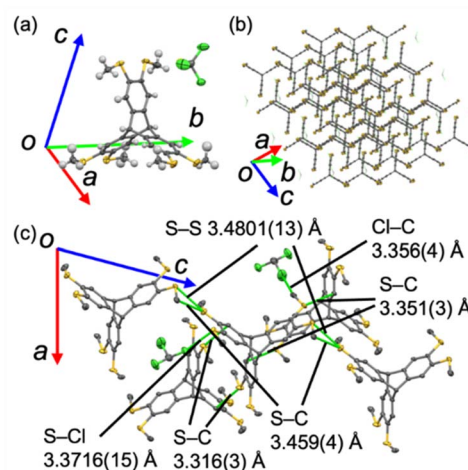

Fig. 2 Crystal structure of HMTTC. (a) Crystal compositions. (b) Packing structure viewed from the axial direction of HMTTC. (c) Short contacts between non-hydrogen atoms around HMTTC. Thermal ellipsoids are set at the 50% probability level. Hydrogen atoms are omitted for simplicity in (b and c).
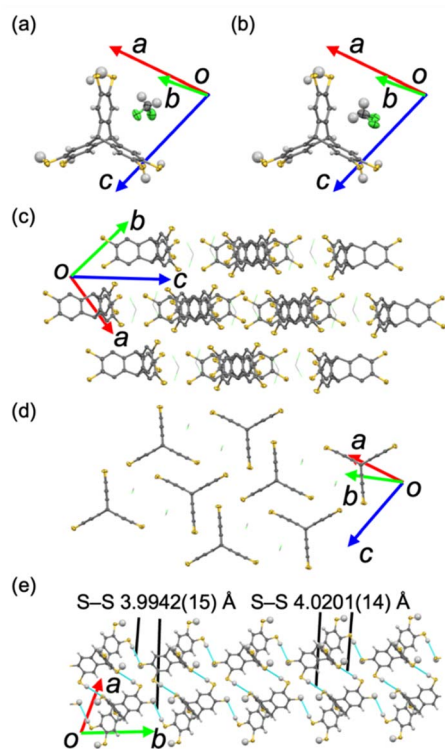
25726 | *J. Mater. Chem. A*, 2025, **13**, 25724–25731

This journal is © The Royal Society of Chemistry 2025

Fig. 3 Crystal structure of TCHT. Crystal compositions with the (a) major and (b) minor conformation of dichloromethane. (c) TCHT molecular stacking in (c) transverse and (d) axial views. (e) Hydrogen bonding network of TCHT. Thermal ellipsoids are set at the 50% probability level. Hydrogen atoms are omitted for simplicity in (c and d).

the contact between the Cl atom and the methyl group (Cl–C: 3.356(4) Å), all the contacts involved S atoms (S–Cl: 3.3716(15) Å; S–S 3.4801(13) Å; S–C: 3.351(3) Å; S–C: 3.316(3) Å; S–C: 3.459(4) Å).

TCHT and dichloromethane were crystallized in 1 : 1 ratio. Both molecules were crystallographically independent with the dichloromethane being disordered in a ratio of 60 : 40 (Fig. 3a and b). The crystal has a layered structure with two dichloromethanes surrounded by two TCHT in each layer (Fig. 3c and d). Although no short contact between non-hydrogen atoms was observed, the presence of interlayer weak hydrogen bonds[54] S···H–S was suggested as shown in Fig. 3e. Hydrogen bonds based on the longer S···H–S (S–S: 4.0201(14) Å) formed the TCHT dimer, while hydrogen bonds based on the shorter S···H–S (S–S: 3.9942(15) Å) formed a one-dimensional hydrogen-bonded chain consisting of TCHT dimers.

Synthesis and characterization of Cu-TCHT

Cu-TCHT was obtained as a black powder sample by adding the methanol solution of Cu(II) acetate monohydrate into the dichloromethane solution of TCHT. Raman spectra of Cu-TCHT (Fig. 4a) exhibited the appearance of ν(Cu–S) stretching at 370 cm^{-1} and the disappearance of ν(S–H) at 2530 cm^{-1}, indicating the complex formation. This assignment was also supported by the infrared spectra of Cu-TCHT (Fig. 4b), which exhibited the disappearance of ν(S–H) stretching at 2530 cm^{-1}. The energy-dispersive X-ray spectrum (EDS) elemental mapping suggests a homogeneous distribution of C, S, and Cu on the Cu-
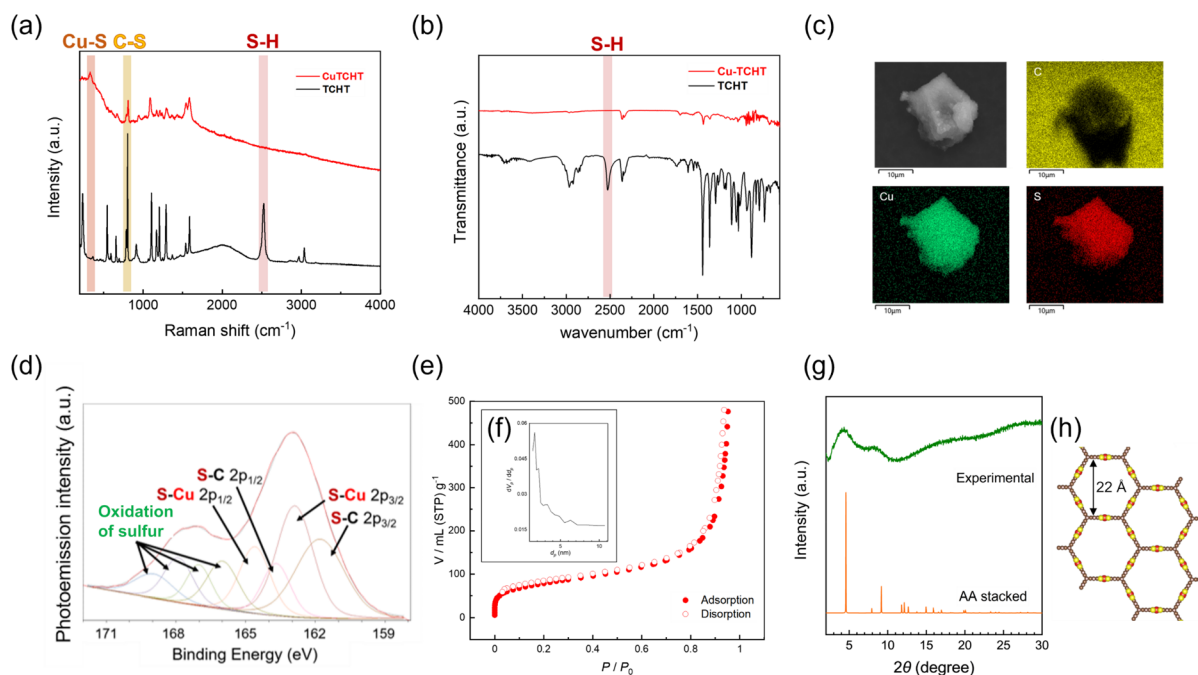

Fig. 4 (a) Raman spectra of TCHT ligand (black) and Cu-TCHT (red). (b) FT-IR spectra of TCHT ligand (black) and Cu-TCHT (red). (c) EDS elemental mapping analysis of Cu-TCHT. (d) XPS S 2p spectrum of Cu-TCHT; red curve represents the experimental value excluding background corrected by the Tougaard method, other color curves represent various bonds and states in the experimental value fitted by the analysis software. (e) N$_2$ sorption properties of Cu-TCHT. (f) Pore size distribution. (g) Experimental and simulated (AA stacked) PXRD patterns of Cu-TCHT. (h) Plausible honeycomb structure of Cu-TCHT.

This journal is © The Royal Society of Chemistry 2025

J. Mater. Chem. A, 2025, **13**, 25724–25731 | **25727**

TCHT (Fig. 4c). X-ray photoelectron spectroscopy (XPS) measurements were performed to investigate the detailed structure of the coordination sites in Cu-TCHT. The full spectrum verifies the existence of copper and sulfur (Fig. S3†). Also, high-resolution XPS measurements were performed for copper and sulfur. The spectra for S (2p) and Cu (2p) of Cu-TCHT are shown in Fig. 4d and Table S3, and in Fig. S4,† respectively. S (2p) spectrum could be deconvoluted in several peaks at 161.8 eV, 162.9 eV, 163.7 eV and 164.5 eV, representing S–C $2p_{3/2}$, S–Cu $2p_{3/2}$, S–C $2p_{1/2}$, and S–Cu $2p_{1/2}$, respectively.[55] This also confirmed that TCHT is coordinated with copper ions. In addition, a peak originating from oxidation of sulfur was observed above 165 eV.[56,57] This is presumably due to the air oxidation of the thiol group, which is commonly observed in the various thiolate based MOFs.[58–60] In the Cu 2p XPS spectrum, the signals at 933.4 eV and 953.2 eV were separately assigned to Cu^{2+} $2p_{3/2}$ and Cu^{2+} $2p_{1/2}$, while the peaks at around 800 eV were assigned to the satellite features of Cu^{2+}. Consequently, it was inferred that the valence of Cu is divalent.[61] The electron paramagnetic resonance (EPR) spectrum of Cu-TCHT displays a broad signal at $g = 2.14$ (Fig. S5†). This is a typical signal from the unpaired electron at $d_{x^2-y^2}$ orbital attributed to square planar Cu(II) complexes. The porosity was evaluated by the N_2 sorption isotherm at 77 K. Cu-TCHT exhibited moderate N_2 adsorption at 77 K, indicating the porosity of the material (Fig. 4e). The pore size distribution showed the relatively large micropores in a diameter of 1.67 nm (Fig. 4f), which was consistent with the calculated porous diameter in the structural model described later.

Powder X-ray diffraction (PXRD) measurements were performed on Cu-TCHT. The PXRD pattern of the as-synthesized Cu-TCHT exhibited broad diffraction peaks at 4.3° and 8.5° (Fig. 4(g)), corresponding to d-spacings of approximately 20 Å and 10 Å, respectively. A model structure based on a hexagonal lattice (Fig. 4(h)) showed a periodicity of approximately 22 Å, and the simulated pattern assuming AA (eclipsed) stacking showed good agreement with the experimental pattern. These results support the proposed honeycomb structure of Cu-TCHT. Further improvement of the crystallinity is necessary for more detailed structural analysis.
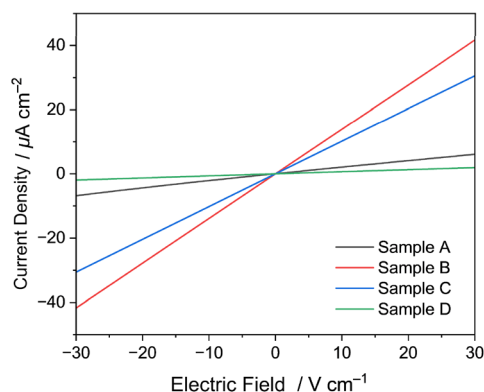
Electrical conductivity of Cu-TCHT synthesized in the glovebox but collected by filtration in air (Sample A) was measured with the two-probe method with the compressed pellet sample at 20 °C (Fig. 5). Cu-TCHT showed the electrical conductivity (σ) of 4.3×10^{-7} S cm^{-1}, which was not high compared to the conventional conductive MOFs. However, it is approximately twice that of Cu-HHTC, a vertical 2D-c-MOF with the oxygen coordination sites instead of sulfur,[42] and about 20 times higher than that of Cu-HTTP with low crystallinity.[60]

As mentioned above, XPS measurements of this MOF revealed peaks corresponding to partial oxidation of sulfur by atmospheric oxygen. Although such ligand oxidation has been commonly observed in similar MOFs,[58–60] to our knowledge, its influence on physical properties has not been investigated to date. Therefore, in this study, we examined the effect of different synthetic and measurement atmospheres on the electrical conductivity. Conductivity measurements were performed under three additional conditions: (i) a sample synthesized and measured entirely in an Ar-filled glovebox (Sample B); (ii) Sample B further treated under vacuum at 120 °C for 24 hours to remove lattice solvents and measured in the glovebox (Sample C); and (iii) a sample exposed to air for one day after synthesis (Sample D). The results showed that both Sample B and Sample C (not exposed to air) exhibited conductivities on the order of 10^{-6} S cm^{-1}, whereas Sample D (exposed to air) showed a conductivity one order of magnitude lower (10^{-7} S cm^{-1}), comparable to Sample A (collected and measured in air) (Fig. 5). These results indicate that the electrical conductivity is not significantly affected by the presence of lattice solvents, but rather by whether the sample has been exposed to air.

This finding suggests that sulfur oxidation may influence electrical conductivity. However, suppression of conductivity by air exposure has also been reported in studies of organic field-effect transistors (trap of the electron carrier).[62] Further investigation is needed to clarify the underlying mechanism of the oxygen-induced effects observed in this MOF.

Meanwhile, the conductivity is still relatively low even under inert conditions (10^{-6} S cm^{-1}), implying that the carrier mobility itself is not very high. We attribute this to the disrupted π-conjugation caused by the sp^3 carbon atoms in the triptycene unit. Nevertheless, for catalytic applications, the lower conductivity can be compensated by incorporating conductive additives, and the improved accessibility to the metal centres offered by this MOF may actually be advantageous.

CO$_2$RR electrocatalytic performance

As mentioned above, 2D-c-MOFs have attracted attention as a promising material for electrocatalysts due to their porosity and high electrical conductivity.[63] Thus, Cu-TCHT is advantageous as an electrocatalyst for CO$_2$ reduction reaction (CO$_2$RR) because of its electrical conductivity and nanosized pores that facilitate rapid mass transport during reactions.

Here, the electrocatalytic activity of Cu-TCHT for the electrochemical reduction of CO$_2$ was demonstrated. The reaction setup is shown in Fig. 6a, and the experimental detail is

Fig. 5 IV characteristics of Cu–TCHT at 20 °C. Sample A: filtered in air, Sample B: synthesized in argon, Sample C: activated *in vacuo* for 24 h at 120 °C, Sample D: exposed in air for 24 h.

25728 | *J. Mater. Chem. A*, 2025, **13**, 25724–25731
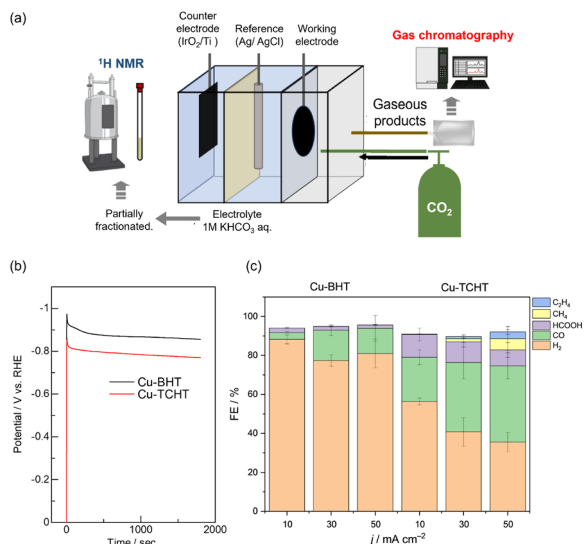
This journal is © The Royal Society of Chemistry 2025

Fig. 6 (a) Reaction setup for evaluation of e-CO_2RR catalytic property. (b) Reaction potential for constant current electrolysis at 10 mA cm^{-2}. (c) Faradaic efficiency for the each product generation using Cu-TCHT and Cu-BHT, whereby error bars represent the standard deviation of independent three experiments.

described in ESI.† Cu-TCHT was loaded on a porous carbon support, Maxsorb, and the composite (Cu-TCHT@Maxsorb) was applied on a carbon electrode. Similarly, Cu-BHT@Maxsorb was prepared for comparison. With the assistance of Maxsorb, Cu-TCHT@Maxsorb exhibited electrical conductivity comparable to that of Cu-BHT@Maxsorb (Fig. S6†).

The potential during the electrolysis were shown in Fig. 6b (10 mA cm^{-2}) and Fig. S7† (30 and 50 mA cm^{-2}). Constant current electrolysis at 10 mA cm^{-2} showed stable performance with an average potential of −0.75 V and −0.87 V for Cu-TCHT@Maxsorb and Cu-BHT@Maxsorb, respectively, which indicates that the Cu-TCHT undergoes the electrolysis with smaller overpotential than Cu-BHT. Fig. 6c shows the faradaic efficiencies (FE) for the main products of CO_2RR. Both of Cu-TCHT@Maxsorb and Cu-BHT@Maxsorb showed CO_2RR catalytic activity and carbon monoxide (CO), formic acid (HCOOH), and very small amount of methane (CH_4) were produced. The total FE of the CO_2 reduction from Cu-TCHT was over 30%, while that from Cu-BHT was only 7%, (Fig. 6c). These findings clearly demonstrate the superior CO_2RR activity in Cu-TCHT with the vertical ligands, probably due to the improved accessibility of the guest molecules to the metal centre.

Conclusions

In conclusion, we synthesized the novel vertical ligand TCHT, determined its crystal structure, and constructed a two-dimensional c-MOF using TCHT. Cu-TCHT was shown to adopt a honeycomb 2D-sheet architecture. Furthermore, Cu-TCHT exhibited high catalytic activity for CO_2 reduction, producing CO, HCOOH, CH_4 and C_2H_4. This study introduces a new class of thiol-functionalized vertical ligands, and we anticipate that various modifications based on this work will

lead to the development of highly functional materials incorporating such ligands.

Data availability

The data supporting this article have been included as part of the ESI.†

Author contributions

W. M. wrote the paper together with Y. C., T. K., R. T., R. S. and S. T. The synthesis and measurements were performed by W. M. and R. S. CO_2RR performance was measured by H. M. and K. I. Data analyses were performed by W. M., Y. C. and T. K., S. T and R. S. directed the project.

Conflicts of interest

There are no conflicts to declare.

Acknowledgements

Notes and references

1 H.-C. Zhou, J. R. Long and O. M. Yaghi, *Chem. Rev.*, 2012, **112**, 673–674.

2 S. R. Batten, N. R. Champness, X.-M. Chen, J. Garcia-Martinez, S. Kitagawa, L. Öhrström, M. O'Keeffe, M. Paik Suh and J. Reedijk, *Pure Appl. Chem.*, 2013, **85**, 1715–1724.

3 L. J. Murray, M. Dincă and J. R. Long, *Chem. Soc. Rev.*, 2009, **38**, 1294.

4 H. Li, K. Wang, Y. Sun, C. T. Lollar, J. Li and H.-C. Zhou, *Mater. Today*, 2018, **21**, 108–121.

5 H. Furukawa, K. E. Cordova, M. O'Keeffe and O. M. Yaghi, *Science*, 2013, **341**, 1230444.

6 R.-B. Lin, S. Xiang, W. Zhou and B. Chen, *Chem*, 2020, **6**, 337–363.

7 Q. Qian, P. A. Asinger, M. J. Lee, G. Han, K. Mizrahi Rodriguez, S. Lin, F. M. Benedetti, A. X. Wu, W. S. Chi and Z. P. Smith, *Chem. Rev.*, 2020, **120**, 8161–8266.

8 L. Jiao, Y. Wang, H. Jiang and Q. Xu, *Adv. Mater.*, 2018, **30**, 1703663.

9 Q. Yang, Q. Xu and H.-L. Jiang, *Chem. Soc. Rev.*, 2017, **46**, 4774–4808.

10 J. L. Obeso, J. G. Flores, C. V. Flores, M. T. Huxley, J. A. De Los Reyes, R. A. Peralta, I. A. Ibarra and C. Leyva, *Chem. Commun.*, 2023, **59**, 10226–10242.

11 A. Schneemann, V. Bon, I. Schwedler, I. Senkovska, S. Kaskel and R. A. Fischer, *Chem. Soc. Rev.*, 2014, **43**, 6062–6096.

This journal is © The Royal Society of Chemistry 2025

J. Mater. Chem. A, 2025, **13**, 25724–25731 | **25729**

12 L. E. Kreno, K. Leong, O. K. Farha, M. Allendorf, R. P. Van Duyne and J. T. Hupp, *Chem. Rev.*, 2012, **112**, 1105–1125.

13 G. Cai, P. Cui, W. Shi, S. Morris, S. N. Lou, J. Chen, J. Ciou, V. K. Paidi, K. Lee, S. Li and P. S. Lee, *Adv. Sci.*, 2020, **7**, 1903109.

14 L. S. Xie, G. Skorupskii and M. Dincă, *Chem. Rev.*, 2020, **120**, 8536–8580.

15 M. Hmadeh, Z. Lu, Z. Liu, F. Gándara, H. Furukawa, S. Wan, V. Augustyn, R. Chang, L. Liao, F. Zhou, E. Perre, V. Ozolins, K. Suenaga, X. Duan, B. Dunn, Y. Yamamto, O. Terasak and O. M. Yaghi, *Chem. Mater.*, 2012, **24**, 3511–3513.

16 T. Kambe, R. Sakamoto, K. Hoshiko, K. Takada, M. Miyachi, J.-H. Ryu, S. Sasaki, J. Kim, K. Nakazato, M. Takata and H. Nishihara, *J. Am. Chem. Soc.*, 2013, **135**, 2462–2465.

17 D. Sheberla, L. Sun, M. A. Blood-Forsythe, S. Er, C. R. Wade, C. K. Brozek, A. Aspuru-Guzik and M. Dincă, *J. Am. Chem. Soc.*, 2014, **136**(25), 8859–8862.

18 X. Huang, P. Sheng, Z. Tu, F. Zhang, J. Wang, H. Geng, Y. Zou, C. Di, Y. Yi, Y. Sun, W. Xu and D. Zhu, *Nat. Commun.*, 2015, **6**, 7408.

19 R. Dong, M. Pfeffermann, H. Liang, Z. Zheng, X. Zhu, J. Zhang and X. Feng, *Angew. Chem., Int. Ed.*, 2015, **54**, 12058–12063.

20 N. Lahiri, N. Lotfizadeh, R. Tsuchikawa, V. V. Deshpande and J. Louie, *J. Am. Chem. Soc.*, 2017, **139**(1), 19–22.

21 J. Park, A. C. Hinckley, Z. Huang, D. Feng, A. A. Yakovenko, M. Lee, S. Chen, X. Zou and Z. Bao, *J. Am. Chem. Soc.*, 2018, **140**, 14533–14537.

22 R. W. Day, D. K. Bediako, M. Rezaee, L. R. Parent, G. Skorupskii, M. Q. Arguilla, C. H. Hendon, I. Stassen, N. C. Gianneschi, P. Kim and M. Dincă, *ACS Cent. Sci.*, 2019, **5**, 1959–1964.

23 G. Skorupskii, B. A. Trump, T. W. Kasel, C. M. Brown, C. H. Hendon and M. Dincă, *Nat. Chem.*, 2020, **12**, 131–136.

24 M. Wang, R. Dong and X. Feng, *Chem. Soc. Rev.*, 2021, **50**, 2764–2793.

25 X. Wang, R. A. Borse, G. Wang, Z. Xiao, H. Zhu, Y. Sun, Z. Qian, S. Zhong and R. Wang, *Mater. Today Energy*, 2024, **44**, 101652.

26 D. Sheberla, J. C. Bachman, J. S. Elias, C.-J. Sun, Y. Shao-Horn and M. Dinca, *Nat. Mater.*, 2017, **16**, 220.

27 F. Deng, Y. Zhang and Y. Yu, *Batteries*, 2023, **9**, 109.

28 C. Park, J. B. Won, E. Shin and I.-D. Kim, *ACS Nanosci. Au*, 2023, **3**, 353–374.

29 M. Ko, L. Mendecki, A. M. Eagleton, C. G. Durbin, R. M. Stolz, Z. Meng and K. A. Mirica, *J. Am. Chem. Soc.*, 2020, **142**, 11717–11733.

30 N. Kornienko, Y. Zhao, C. S. Kley, C. Zhu, D. Kim, S. Lin, C. J. Chang, O. M. Yaghi and P. Yang, *J. Am. Chem. Soc.*, 2015, **137**, 14129–14135.

31 T. Zhan, Y. Zou, Y. Yang, X. Ma, Z. Zhang and S. Xiang, *ChemCatChem*, 2022, **14**, e202101453.

32 Z. H. Syed, F. Sha, X. Zhang, D. M. Kaphan, M. Delferro and O. K. Farha, *ACS Catal.*, 2020, **10**, 11556–11566.

33 A. Bavykina, N. Kolobov, I. S. Khan, J. A. Bau, A. Ramirez and J. Gascon, *Chem. Rev.*, 2020, **120**, 8468–8535.

34 W. Tu, Y. Xu, S. Yin and R. Xu, *Adv. Mater.*, 2018, **30**, 1707582.

35 D. A. Reed, D. J. Xiao, M. I. Gonzalez, L. E. Darago, Z. R. Herm, F. Grandjean and J. R. Long, *J. Am. Chem. Soc.*, 2016, **138**, 5594–5602.

36 D. E. Jaramillo, H. Z. H. Jiang, H. A. Evans, R. Chakraborty, H. Furukawa, C. M. Brown, M. Head-Gordon and J. R. Long, *J. Am. Chem. Soc.*, 2021, **143**, 6248–6256.

37 K. Baumgärtner, M. Hoffmann, R. Frank, S. M. Elbert, A. Dreuw and M. Mastalerz, *J. Org. Chem.*, 2020, **85**, 15256–15272.

38 K. Ohno, T. Ishida, Y. Naitoh and Y. Izumi, *J. Am. Chem. Soc.*, 1985, **107**, 8082–8086.

39 K. Kawasumi, T. Wu, T. Zhu, H. S. Chae, T. Van Voorhis, M. A. Baldo and T. M. Swager, *J. Am. Chem. Soc.*, 2015, **137**, 11908–11911.

40 K. S. Song, D. Kim, K. Polychronopoulou and A. Coskun, *ACS Appl. Mater. Interfaces*, 2016, **8**, 26860–26867.

41 J. Lv, W. Li, J. Li, Z. Zhu, A. Dong, H. Lv, P. Li and B. Wang, *Angew. Chem., Int. Ed.*, 2023, **62**, e202217958.

42 Y. Shuku, R. Suizu, M. Tsuchiizu and K. Awaga, *Chem. Commun.*, 2023, **59**, 10105–10108.

43 H. Maeda, Y. Sudo, S. Nagashima, K. Takada, N. Fukui, H. Masunaga, S. Sasaki and H. Nishihara, *ACS Appl. Nano Mater.*, 2024, **7**, 13775–13784.

44 G. Wittig, in *Organic Syntheses*, ed. A. S. Kende and J. P. Freeman, Wiley, 1st edn, 2003, pp. 75.

45 Y. Chiba, T. Tanabe, K. Koizumi, R. Toyoda, H. Iguchi, S. Takaishi and R. Sakamoto, *Inorg. Chem.*, 2023, **62**, 11731–11736.

46 C. L. Hilton, C. R. Jamison, H. K. Zane and B. T. King, *J. Org. Chem.*, 2009, **74**, 405–407.

47 P. Chakma and D. Konkolewicz, *Angew. Chem., Int. Ed.*, 2019, **58**, 9682–9695.

48 S. P. Black, J. K. M. Sanders and A. R. Stefankiewicz, *Chem. Soc. Rev.*, 2014, **43**, 1861.

49 Q. Zhang, D.-H. Qu, B. L. Feringa and H. Tian, *J. Am. Chem. Soc.*, 2022, **144**, 2022–2033.

50 S. Otto, R. L. E. Furlan and J. K. M. Sanders, *Science*, 2002, **297**, 590–593.

51 Y. Deng, Q. Zhang, C. Shi, R. Toyoda, D.-H. Qu, H. Tian and B. L. Feringa, *Sci. Adv.*, 2022, **8**, eabk3286.

52 A. M. Richter, V. Engels, N. Beye and E. Fanghänel, *Z. Chem.*, 1989, **29**, 444–445.

53 H. K. Yip, A. Schier, J. Riede and H. Schmidbaur, *J. Chem. Soc., Dalton Trans.*, 1994, **15**, 2333–2334.

54 G. R. Desiraju and T. Steiner, *The Weak Hydrogen Bond: in Structural Chemistry and Biology*, Oxford University Press, Oxford, 1999.

55 Y. Wu, Y. Luo, P. K. Chu and C. Menon, *Nano Energy*, 2023, **111**, 108427.

56 S. M. Islam, V. K. Sangwan, Y. Li, J. Kang, X. Zhang, Y. He, J. Zhao, A. Murthy, S. Ma, V. P. Dravid, M. C. Hersam and M. G. Kanatzidis, *ACS Appl. Mater. Interfaces*, 2018, **10**, 38193–38200.

57 T. Islam, M. Li, A. Blanton, K. A. Pitton, K. R. Rao, S. Bayat, K. M. Wiaderek, M. A. Weret, S. C. Roy, R. Feng, D. Li, R. Alam, J. Nie, O. Oketola, A. Pramanik, B. S. Guiton,

25730 | *J. Mater. Chem. A*, 2025, **13**, 25724–25731

This journal is © The Royal Society of Chemistry 2025

C. Risko, I. Belharouak, R. Amin and S. M. Islam, *ACS Energy Lett.*, 2024, **9**, 1–9.

58 J. Guan, K. Koizumi, N. Fukui, H. Suzuki, K. Murayama, R. Toyoda, H. Maeda, K. Kamiya, K. Ohashi, S. Takaishi, O. Tomita, A. Saeki, H. Nishihara, H. Kageyama, R. Abe and R. Sakamoto, *ACS Catal.*, 2024, **14**, 1146–1156.

59 R. Dong, P. Han, H. Arora, *et al.*, *Nat. Mater.*, 2018, **17**, 1027–1032.

60 L. Mendecki, M. Ko, X. Zhang, Z. Meng and K. A. Mirica, *J. Am. Chem. Soc.*, 2017, **139**, 17229–17232.

61 J. Conradie and E. Erasmus, *J. Electron Spectrosc. Relat. Phenom.*, 2022, **259**, 147241.

62 J. Zaumseil and H. Sirringhaus, *Chem. Rev.*, 2007, **107**, 1296–1323.

63 T. Zhan, Y. Zou, Y. Yang, X. Ma, Z. Zhang and S. Xiang, *ChemCatChem*, 2022, **14**, e202101453.

This journal is © The Royal Society of Chemistry 2025

J. Mater. Chem. A, 2025, **13**, 25724–25731 | **25731**